Struct Multidisc Optim
DOI 10.1007/s00158-011-0636-9

RESEARCH PAPER

# Reduced representations of vector-valued coupling variables in decomposition-based design optimization

**Michael J. Alexander · James T. Allison · Panos Y. Papalambros**

Received: 28 August 2010 / Revised: 3 January 2011 / Accepted: 9 February 2011


**Abstract** Decomposition-based optimization strategies decouple a system design problem and introduce coupling variables as decision variables that manage communication among subproblems. The computational cost of such approaches is comparable to that of the equivalent, yet usually unsuccessful, attempts to solve the coupled system directly when the coupling variables consist of a small, finite number of scalars. When the coupling variables are infinite-dimensional quantities, such as functional data, implementing decomposition-based optimization strategies may become computationally challenging. Discretization is typically applied, transforming infinite-dimensional variables into finite-dimensional ones represented as vectors. A large number of discretized points is often necessary to ensure a sufficiently accurate representation of the functional data, and so the dimensionality of these vector-valued coupling variables (VVCVs) can become prohibitively large for decomposition-based design optimization. Therefore, it is desirable to approximate the VVCVs with a reduced dimension representation that improves optimization efficiency while preserving sufficient accuracy. We investigate two VVCV representation techniques, radial-basis function artificial neural networks and proper orthogonal decomposition, and implement each in an analytical target cascading problem formulation for electric vehicle powertrain system optimization. Specifically, both techniques are applied to VVCVs associated with motor boundary torque curves and power loss maps and are assessed in terms of dimensionality reduction, computational expense, and accuracy.

**Keywords** Decomposition-based design optimization · Analytical target cascading · Coupling variables · Dimensionality · Reduced representation · Vector-valued target

## 1 Introduction

The complexity of modern, large-scale system design is often a result of the highly-coupled nature of the subsystems and components comprising the overall system. In the context of design optimization, complexity and size can prohibit efficient or reliable solution of a single system formulation, and therefore decomposition-based optimization strategies are employed (Allison 2008; Wagner and Papalambros 1993). In these strategies, the coupling variables communicated between subproblems are treated as decision variables. In the absence of special problem structure, such as sparsity, the computational cost of the increased dimensionality is a necessary by-product of these strategies. When the coupling variables are just a few, finite scalars, this extra cost is negligible. However, when the coupling variables are infinite-dimensional quantities, such as functional data, decomposition-based strategies may become very expensive computationally. Discretization is typically applied, transforming infinite-dimensional variables into finite-dimensional ones, which can be represented in vector form as

$$z = f(y) \approx F\left(\left[z_1,\ z_2, \cdots,\ z_q\right]^T, \left[y_1,\ y_2, \cdots,\ y_q\right]^T, y\right) \quad (1)$$

Originally presented at WCSMO-8.

M. J. Alexander (✉) · P. Y. Papalambros
Department of Mechanical Engineering, University of Michigan, Ann Arbor, MI 48104, USA
e-mail: malexanz@umich.edu

J. T. Allison
The MathWorks, Inc., Natick, MA 01760, USA

Published online: 31 March 2011

where $y$ is the independent variable, $z$ is the dependent variable, $q$ is the number of discretized points, and $F$ is some type of interpolation function, such as a lookup table. Although this transformation enables quantities that are functions of infinite-dimensional coupling variables to be computed, it often requires a large number of discretized points to ensure a sufficiently accurate representation of the functional data. In such cases, the dimensionality (given by $q$) of these vector-valued coupling variables (VVCVs) can become prohibitively large for decomposition-based design optimization. Therefore, it is desirable to approximate the VVCVs with a reduced dimension representation that improves optimization efficiency while preserving sufficient accuracy. The alternative set of coupling variables comprising these reduced representations are referred to as reduced representation variables (Alexander 2008; Alexander et al. 2009).

The published literature addressing the problem of representing VVCVs in decomposition-based optimization strategies is fairly limited. Sobieski and Kroo (1996) experienced reasonable success using Fourier coefficients to represent a lift distribution generated by an aerodynamics subproblem in the design of an aircraft within a collaborative optimization (CO) framework. However, there was no explicit indication why this method was sufficient for this work as this was not the main theme of the paper; rather, the authors were attempting to demonstrate the capability of CO. Meade and Kokkolaras (1996) addressed this issue from the broader perspective of analysis in the solution of a viscous-inviscid-interaction airfoil analysis code. In this case, linear combinations of quadratic polynomials were used to approximate transpiration velocity vectors exchanged between underlying coupled analysis functions that were solved iteratively. Like the previous authors, however, the dimensionality reduction problem was not the primary focus of the paper, and therefore, there was limited information regarding the motivation for selecting the method. Finally, LeGresley and Alonso (2004) used proper orthogonal decomposition (POD) to represent surface pressure and structural displacement distributions generated by aerodynamics and structural subproblems in the optimization of a low-fidelity aeroelastic model within a bi-level integrated system synthesis (BLISS) framework. Although the authors produced promising results, they also acknowledged the need to demonstrate the effectiveness of POD in a more compelling problem that contained higher-fidelity models.

The particular motivating application for the present work is the use of analytical target cascading (ATC) for hybrid-electric vehicle (HEV) powertrain system optimization. In early unpublished work on this problem, it was necessary to reduce the dimensionality of VVCVs associated with maximum and minimum motor/generator torque curves and power loss maps. Polynomial response surface approximation (Box and Hunter 1957; Box and Draper 1987; George and Ogot 2006) was initially implemented, with the polynomial coefficients serving as reduced representation variables. However, this was deemed ineffective as many coefficients were required to produce approximations of reasonable accuracy. In a more heuristic approach, weight coefficients were used as reduced representation variables in the linear interpolation of two distinct "baseline" functions to approximate the original representations. While this technique significantly reduced the dimensionality of the VVCVs, the accuracy of the new representations was significantly compromised. Weight coefficients were again used in linear combinations of orthogonal functions (Bretscher 2005; Sansone and Hille 2004) to approximate the original representations. Because orthogonality conditions were not strictly enforced, this method was somewhat heuristic in its implementation; nevertheless, the fundamental concept behind this method was similar to POD, which indicated some promise. Image warping (Stegmann 2001; Glasbey and Mardia 1998), which used warping parameters as reduced representation variables, also demonstrated some efficacy but it was challenging to determine appropriate transformations for the motor curves and map. Based on an earlier, related ATC study (Kokkolaras et al. 2004), implementing radial-basis function (RBF) artificial neural networks (ANN) with input variables serving as reduced representation variables appeared to be a promising approach due to its high accuracy.

This paper examines the implementation of RBF ANN and POD in the optimization of an electric vehicle (EV) powertrain system using ATC. Section 2 reviews ATC briefly; Section 3 discusses the reduced representations using RBF ANN and POD; Section 4 presents a summary of the vehicle model; Sections 5 and 6 present results and their assessment, respectively; and Section 7 offers some conclusions.

## 2 Review of analytical target cascading

ATC (Kim 2001; Kim et al. 2003) is a hierarchical, decomposition-based optimization strategy for large-scale systems that minimizes performance-related objectives local to each subproblem while minimizing deviations between design targets cascaded from upper levels and their realizable responses at lower levels. An optimal system solution is achieved when the targets and responses are consistent, or in agreement, with one another.

The strategy begins by first decomposing the system into design subproblems such that the top level is known as the

system level and lower levels are known as subsystem levels. Note that a subproblem linked above a given element of interest is called a parent, and those subproblems linked below a given element of interest are called children. The general ATC subproblem $P_{ij}$ for the *ith* level and the *jth* element can be defined as (Tosserams et al. 2006):

$$\begin{aligned} &\min_{\bar{\mathbf{x}}_{ij}} f_{ij}\left(\bar{\mathbf{x}}_{ij}\right) + \pi\left(\mathbf{c}\left(\bar{\mathbf{x}}_{11}, \cdots, \bar{\mathbf{x}}_{NM}\right)\right) \\ &\text{subject to} \quad \mathbf{g}_{ij}\left(\bar{\mathbf{x}}_{ij}\right) \leq \mathbf{0}, \mathbf{h}_{ij}\left(\bar{\mathbf{x}}_{ij}\right) = \mathbf{0} \\ &\text{where} \quad \bar{\mathbf{x}}_{ij} = \left[\mathbf{x}_{ij},\ \mathbf{r}_{ij},\ \mathbf{t}_{(i+1)k_1}, \cdots,\ \mathbf{t}_{(i+1)k_{c_{ij}}}\right], \\ &\mathbf{c} = \left[\mathbf{c}_{22}, \cdots,\ \mathbf{c}_{NM}\right] \end{aligned} \tag{2}$$

In the above, $\mathbf{x}_{ij}$ is the vector of local design variables, $\mathbf{t}_{ij}$ is the vector of target linking variables passed from the element's parent at level $(i-1)$, $\mathbf{r}_{ij}$ is the vector of response linking variables passed to the element's parent at level $(i-1)$, $\mathbf{c}_{ij} = \mathbf{t}_{ij} - \mathbf{r}_{ij}$ is the vector of consistency constraints between target and response linking variables, $f_{ij}$ is the local objective function, $\pi$ is the penalty function, $\mathbf{g}_{ij}$ is the vector of inequality constraints, $\mathbf{h}_{ij}$ is the vector of equality constraints, $N$ is the number of levels, and $M$ is the total number of elements. Although $\mathbf{t}_{ij}$ and $\mathbf{r}_{ij}$ can include both coupling and shared variables, only coupling variables are present in this study. Also, observe that the consistency constraints, which should be zero for an exact system solution, are relaxed through $\pi(\mathbf{c})$ such that $||\mathbf{c}^{(\mathrm{K})} - \mathbf{c}^{(K-1)}||_\infty$ is within some small tolerance before the algorithm is terminated, where $K$ denotes the iteration number.

An augmented-Lagrangian (AL) penalty function was selected for this study and resulted in the following general ATC-AL subproblem formulation for the *ith* level and *jth* element (Tosserams et al. 2006):

$$\begin{aligned} &\min_{\bar{\mathbf{x}}_{ij}} f_{ij}\left(\bar{\mathbf{x}}_{ij}\right) - \mathbf{v}_{ij}^T \mathbf{r}_{ij} \\ &\qquad + \sum_{k \in C_{ij}} \mathbf{v}_{(i+1)k}^T \mathbf{t}_{(i+1)k} + \left\| \mathbf{w}_{ij} \circ \left(\mathbf{t}_{ij} - \mathbf{r}_{ij}\right)\right\|_2^2 \\ &\qquad + \sum_{k \in C_{ij}} \left\| \mathbf{w}_{ij} \circ \left(\mathbf{t}_{(i+1)k} - \mathbf{r}_{(i+1)k}\right)\right\|_2^2 \\ &\text{subject to} \quad \mathbf{g}_{ij}\left(\bar{\mathbf{x}}_{ij}\right) \leq \mathbf{0},\ \mathbf{h}_{ij}\left(\bar{\mathbf{x}}_{ij}\right) = \mathbf{0} \\ &\text{where} \quad \bar{\mathbf{x}}_{ij} = \left[\mathbf{x}_{ij},\ \mathbf{r}_{ij},\ \mathbf{t}_{(i+1)k_1}, \cdots,\ \mathbf{t}_{(i+1)k_{c_{ij}}}\right] \end{aligned} \tag{3}$$

Note that the linear and quadratic terms in the AL penalty function are weighted by the vectors $\mathbf{v}$ and $\mathbf{w}$, respectively. Finally, all subproblems are solved in an inner loop strategy

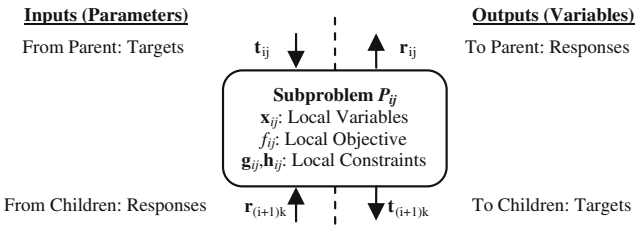


**Fig. 1** ATC information flow (Tosserams et al. 2006)

where the weights remain constant. If the outer loop termination criterion (sufficiently small $||c^{(\mathrm{K})} - c^{(K-1)}||_\infty$) is not met, then the weights are updated accordingly:

$$\begin{aligned} \mathbf{v}^{(K+1)} &= \mathbf{v}^{(K)} + 2\mathbf{w}^{(K)} \circ \mathbf{w}^{(K)} \circ \mathbf{c}^{(K)} \\ \mathbf{w}^{(K+1)} &= \beta \mathbf{w}^{(K)}, \text{ where } \beta \geq 1 \end{aligned} \tag{4}$$

Figure 1 illustrates the information flow for the general ATC-AL subproblem.

## 3 Reduced representations of vector-valued coupling variables

Because RBF ANN is an established method for the representation of VVCVs in decomposition-based optimization strategies, it serves as a "baseline" approach to which POD will be compared. Among the key differences, however, in the implementation of these techniques is that RBF ANN achieves dimensionality reduction through a metamodeling approach, whereas POD achieves dimensionality reduction through a curve-fitting approach. Specifically, the RBF ANN implementation develops a metamodel of the analysis function that relates an input vector containing physical design variables to VVCVs as in Kokkolaras et al. (2004). Since the dimensionality of the input vector is significantly less than the dimensionality of the VVCVs for this study, this approach can be used as a reduced representation. Conversely, the POD implementation establishes a functional form to represent the VVCVs and then varies a set of curve-fitting parameters to sufficiently approximate the original representation. Because the number of curve-fitting parameters is significantly less than the dimensionality of the VVCVs, reduced representation is achieved. RBF ANN is not used in this fashion because in general, the number of curve-fitting parameters required to reasonably approximate the VVCVs would be greater than the dimensionality of the VVCVs. A general flowchart of how these reduced

representation methods should be implemented in ATC is illustrated in Fig. 2.

### 3.1 Radial-basis function artificial neural networks

RBF ANN (Demuth et al. 2009) is a technique that develops a mapping to describe the functional relationship between sample input/output vector pairs $\mathbf{u}_i = [u_1, u_2, \ldots, u_p]^T$ and $\mathbf{z}_i = [z_1, z_2, \ldots, z_q]^T$ for all $i = 1 \ldots m$ samples such that the exact function $\mathbf{z} = \mathbf{f}(\mathbf{u})$ can be approximated at any input vector $\mathbf{u}_j$ in the sampling domain. This mapping is accomplished through a weighted, linear combination of RBFs (Chen et al. 1991; Demuth et al. 2009):

$$\mathbf{z} = \mathbf{f}(\mathbf{u}) \approx \mathbf{g}(\mathbf{u}) = \sum_{k=1}^{n} \phi_{rbf,k}(\mathbf{u})\, \boldsymbol{\omega}_k + \mathbf{b} \tag{5}$$

Here, $\mathbf{g}(\mathbf{u})$ is the approximation of the exact function $\mathbf{f}(\mathbf{u})$, $\phi_{rbf,k}(\mathbf{u})$ is the *kth* RBF, $n$ is the number of RBFs and neurons, $\boldsymbol{\omega}_k$ is the *kth* weight vector, and $\mathbf{b}$ is the bias vector. Because it is assumed that the dimensionality of the input is less than the dimensionality of the output ($p << q$), $\mathbf{u}$ and $\mathbf{z}$ can be regarded as the reduced representation and the original VVCV, respectively. It should be observed that such a reduced representation could have been obtained directly through the use of $\mathbf{f}(\mathbf{u})$; however, this would have contradicted another motivation for ATC. Specifically, ATC is intended to enable the use of lower-fidelity analysis models at upper levels within the decomposition hierarchy and higher-fidelity models at the lower levels. Therefore, since the VVCVs in this problem will be used at the top level of the hierarchy (see Section 5), the reduced representation is obtained through the use of the approximation model $\mathbf{g}(\mathbf{u})$.

Although many different types of RBFs can be used, the one most commonly employed for these neural networks is the Gaussian density function:

$$\phi_{rbf,k}(\mathbf{u}) = e^{-(\|\mathbf{u}-\gamma_k\| b_h)^2} \tag{6}$$

In the above, $\boldsymbol{\gamma}_k$ denotes the center of the *kth* RBF and $b_h$ denotes the hidden layer bias of the neural network. With these two parameters set a priori and using the $m$ sampling pairs, the neural network is typically designed (or "trained") by determining $\boldsymbol{\omega}_k$ and $\mathbf{b}$ such that the error between the exact function and its approximation is minimized in a least-squares sense (Demuth et al. 2009):

$$\|\mathbf{f} - \mathbf{g}\| = \sqrt{\sum_{i=1}^{m} (\mathbf{z}_i - \mathbf{g}(\mathbf{u}_i))^2} \tag{7}$$

Alternatively, a curve-fitting approach could be used for a "customized" RBF ANN that would allow for a more direct comparison to POD. In particular, an RBF ANN architecture could first be established between discretized function inputs in $\mathbf{y}$ and corresponding elements in VVCVs through $m$ sample pairs. From here, $(n+1)$ scalar-valued curve-fitting parameters ($n$ weights plus a bias) could be used as reduced representation variables to approximate any VVCV if $(n+1) << q$. However, a considerable amount of effort would be required to determine such a customized architecture (including the number of RBFs, $\gamma_k$, and $b_h$) for a specific data set, and there would be no guarantee that $(n+1) << q$. This approach is therefore proposed as future work.

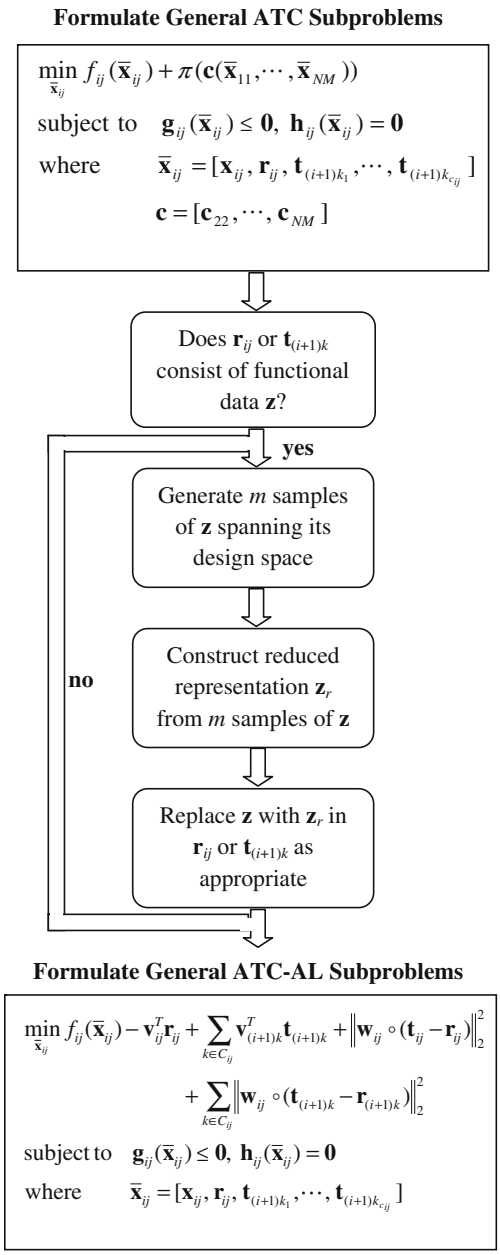


**Fig. 2** Flowchart for reduced representation in ATC

For the EV design study, three RBF ANN were designed to relate input vectors consisting of motor design variables to output vectors consisting of VVCVs associated with maximum and minimum motor torque curves and power loss maps:

$$\mathbf{z}_{max} \approx \mathbf{g}_{max}(\mathbf{u}), \quad \mathbf{z}_{min} \approx \mathbf{g}_{min}(\mathbf{u}), \quad \mathbf{z}_{pLoss} \approx \mathbf{g}_{pLoss}(\mathbf{u}) \tag{8}$$

The motor design variables were based on the EV powertrain system model developed by Allison (2008) and include the stack length $l_s$, rotor radius $r_m$, number of turns per stator coil $n_c$, and rotor resistance $R_r (p = 4)$:

$$\mathbf{u} = [l_s,\ r_m,\ n_c,\ R_r]^T \tag{9}$$

The VVCVs, in turn, were originally determined by processing the motor design variables in a motor simulation within the powertrain model. Each VVCV associated with the torque curves contained $q_{\max} = q_{\min} = 41$ values, whereas the VVCV associated with the power loss map contained $q_{pLoss} = 3321$ values. The set of training input/output vectors was generated through a Latin hypercube sample (LHS) design of experiments for $m = 2500$ samples. Using these training vector pairs, the neural networks were developed in MATLAB® (MATLAB® Function Reference, MathWorks, Inc., Natick, MA) with the *newrbe* function, which modifies (7) by enforcing an exact solution on all training vectors. Note that the training vectors were normalized to enhance the design and performance of the neural networks, which is common practice. Based on inspection, it can be seen that implementing RBF ANN under the strict condition that $p << q$ significantly reduces the combined dimensionality of the VVCVs from $Q = q_{\max} + q_{\min} + q_{pLoss} = 3403$ to $Q = p = 4$.

### 3.2 Proper orthogonal decomposition

POD is often used in engineering applications as a model reduction technique to facilitate the analysis, design, and optimization of dynamic, linear systems. In broader applications, POD is also referred to as principal component analysis (Ahmed and Goldstein 1975) or Karhunen–Loeve expansion (Karhunen 1946; Loeve 1945). Mathematically, all of these terms refer to the same linear transformation method, but with a particular meaning in various fields. POD, in particular, reduces the state-space representation of dynamic systems according to (Wilcox 2005):

$$\mathbf{z}(t) \approx \mathbf{\Phi}_p \mathbf{z}_r(t) + \bar{\mathbf{z}}(t) \tag{10}$$

Here, $\mathbf{z}(t)$ is the original state vector of dimension $q$, $\mathbf{z}_r(t)$ is the reduced state vector of dimension $p << q$, and $\mathbf{\Phi}_p$ is a matrix of the $p$ most energetic basis functions $\boldsymbol{\varphi}$ used to construct the approximation of the original state vector. The final term $\bar{\mathbf{z}}(t)$ is the sample mean vector of dimension $q$ and is used to center the data for the approximation. This transformation can be applied to the current study by treating the VVCVs as state vectors, thus modifying (10) by

$$\mathbf{z} \approx \mathbf{\Phi}_p \mathbf{z}_r + \bar{\mathbf{z}} \tag{11}$$

where $\mathbf{z}$ is the original $q$-dimensional VVCV, $\mathbf{z}_r$ is the $p$-dimensional reduced representation, and $\mathbf{\Phi}_p$ and $\bar{\mathbf{z}}$ have the same meaning as in the state vector context but applied to VVCVs. POD ultimately involves the construction of the full basis function matrix $\mathbf{\Phi}$ based on $m$ samples $\mathbf{z}_i = [z_1, z_2, \ldots, z_q]^T$ and its reduction by examining the magnitude of its associated eigenvalues. This is accomplished by using either the direct method or the "method of snapshots" (Sirovich 1987).

The most efficient approach when $q \leq m$ is the direct method (Burkhardt et al. 2003), which begins by forming the covariance matrix $\mathbf{R}$:

$$\mathbf{R} = \frac{(\mathbf{Z} - \bar{\mathbf{Z}})(\mathbf{Z} - \bar{\mathbf{Z}})^T}{m - 1} \tag{12}$$

In the above, $\mathbf{Z}$ is a $(q \times m)$ matrix containing all the samples of the original VVCV and $\bar{\mathbf{Z}}$ is a $(q \times m)$ matrix of the sample mean vector repeated $m$ times. Next, a $(q \times q)$ eigenvalue problem on $\mathbf{R}$ is used to construct $\mathbf{\Phi}$,

$$\mathbf{R}\mathbf{\Phi} = \mathbf{\Phi}\mathbf{\Lambda} \tag{13}$$

where $\mathbf{\Lambda}$ is the diagonal matrix of eigenvalues. Assuming that the basis functions in $\mathbf{\Phi}$ are arranged according to the magnitude of their associated eigenvalues,

$$\mathbf{\Phi} = \begin{bmatrix} \mathbf{\Phi}_1 & \mathbf{\Phi}_2 & \cdots & \mathbf{\Phi}_q \end{bmatrix}^T,\ \lambda_1 > \lambda_1 > \cdots > \lambda_q \tag{14}$$

this matrix is reduced to $\mathbf{\Phi}_p$ based on the cumulative percentage variation (CPV). The CPV is a measure of the relative importance of each basis function in $\mathbf{\Phi}$ (Toal et al. 2008):

$$\frac{\sum_{i=1}^{p} \lambda_i}{\sum_{i=1}^{q} \lambda_i} \times 100 \geq CPV_{goal} \tag{15}$$

Observe that $CPV_{goal}$ is set based on the desired amount of information to be captured through POD, which is usually 99% (Bui-Thanh et al. 2004).

When $q > m$, the most efficient solution technique (Burkhardt et al. 2003; Lucia et al. 2003; Wilcox 2005) is the "method of snapshots" (Sirovich 1987). This time, a correlation matrix $\mathbf{R}$ is generated:

$$\mathbf{R} = \frac{(\mathbf{Z} - \bar{\mathbf{Z}})^T (\mathbf{Z} - \bar{\mathbf{Z}})}{m} \tag{16}$$

From here, the associated $(m \times m)$ eigenvalue problem is solved,

$$\mathbf{RV} = \mathbf{V\Lambda} \tag{17}$$

where $\mathbf{V}$ represents the matrix of eigenvectors. The $(q \times m)$ orthogonal basis function matrix is constructed from:

$$\mathbf{\Phi} = \mathbf{ZV}_n, \quad v_{n,ij} = \left(1/\sqrt{m\lambda_{ii}}\right) v_{ij} \tag{18}$$

The above equations demonstrate why this procedure is referred to as the "method of snapshots"; each basis function is a linear combination of the $m$ sample vectors, or "snapshots", of original data (Sirovich 1987). Finally, $\mathbf{\Phi}_p$ is determined using the same procedure outlined in (14)–(15) with $q$ replaced by $m$.

For the current study, three POD representations were developed to approximate the VVCVs described in (8):

$$\begin{aligned} \mathbf{z}_{max} &\approx \mathbf{\Phi}_{p,max}\mathbf{z}_{r,max} + \bar{\mathbf{z}}_{max} \\ \mathbf{z}_{min} &\approx \mathbf{\Phi}_{p,min}\mathbf{z}_{r,min} + \bar{\mathbf{z}}_{min} \\ \mathbf{z}_{pLoss} &\approx \mathbf{\Phi}_{p,pLoss}\mathbf{z}_{r,pLoss} + \bar{\mathbf{z}}_{pLoss} \end{aligned} \tag{19}$$

The sample vectors used to construct $\mathbf{\Phi}_p$ in these expressions were identical to those used in the RBF ANN. Because $q_{\max} = q_{\min} << m$, the direct method was used to generate $\mathbf{\Phi}_{p,max}$ and $\mathbf{\Phi}_{p,min}$, whereas the "method of snapshots" was used to generate $\mathbf{\Phi}_{p,pLoss}$ since $q_{pLoss} >> m$.

Note that for this study, $CPV_{goal}$ was set to 99.99%; however, other studies (Alexander et al. 2010a; Alexander 2011) have extensively explored this parameter and its impact on decomposition-based optimization strategies. The resulting POD representations for $\mathbf{z}_{r,max}$, $\mathbf{z}_{r,min}$, and $\mathbf{z}_{r,pLoss}$ had dimensionalities of $p_{max} = 14$, $p_{min} = 13$, and $p_{pLoss} = 96$, respectively. Clearly, it can be seen that POD significantly reduces the individual dimensionality of each VVCV and the combined dimensionality $Q$ from 3403 to $Q = p_{\max} + p_{\min} + p_{pLoss} = 123$.

## 4 Electric vehicle powertrain model

The EV powertrain simulation model used in this study considered is based on Allison (2008) and developed in MATLAB®/Simulink® environment. Figure 3 shows a general plan view of the vehicle, which is a two-passenger, mini-compact (wheelbase $L = 1.80$ m, track width $W = 1.27$ m) intended for urban driving with some highway speed capability. Its energy storage system consists of a lithium-ion battery, which can vary in length, width, and longitudinal location relative to the vehicle front end such that it lies within the dashed region defined by $b_{lmax} = 1.05$ m and width $b_{wmax} = 1.20$ m. The EV is powered by two electric traction motors through a synchronous belt drive system which are mounted at the pivots on the rear

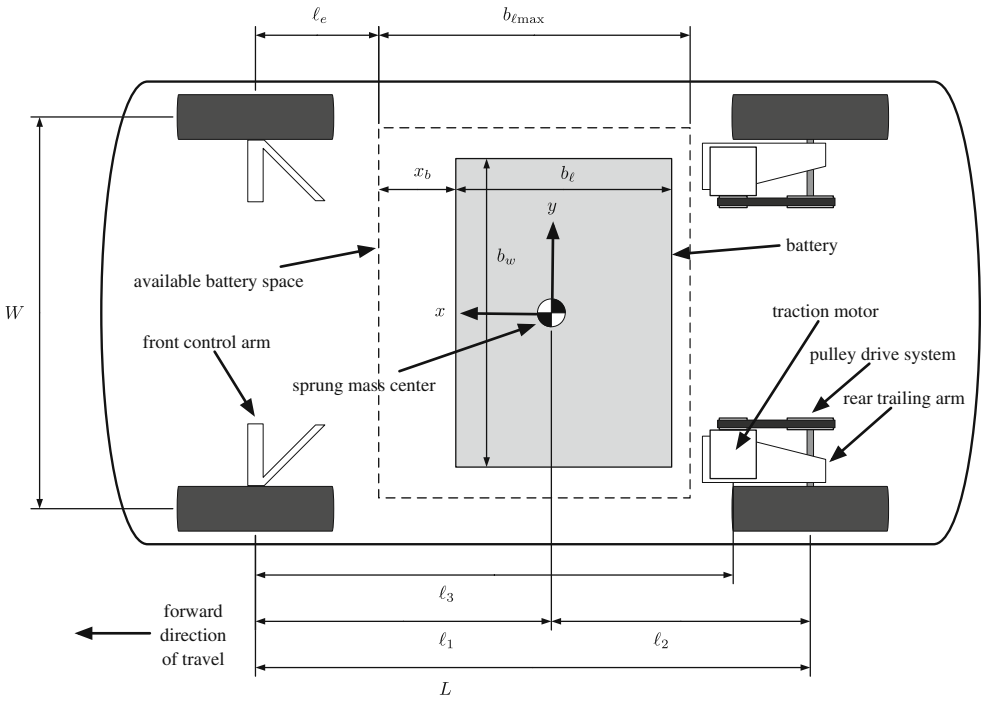


**Fig. 3** General plan view of electric vehicle (Allison 2008)

**Table 1** Definition of input/output quantities to analysis models

| Quantity | Definition | Quantity | Definition |
|---|---|---|---|
| $l_s$ | Motor stack length (m) | $m_s$ | Sprung mass (kg) |
| $r_m$ | Rotor radius (m) | $\ell_1$ | Longitudinal center of mass location (m) |
| $R_r$ | Rotor resistance ($\Omega$) | h | Vertical center of mass location (m) |
| $n_c$ | Number of turns per stator coil | $I_y$ | Pitch moment of inertia (kg-m$^2$) |
| $\mathbf{z}_{max}$ | Max torque VVCV | $I_z$ | Yaw moment of inertia (kg-m$^2$) |
| $\mathbf{z}_{min}$ | Min torque VVCV | $b_{w,V}$ | Battery width violation constraint |
| $\mathbf{z}_{pLoss}$ | Power loss VVCV | $b_{l,V}$ | Battery length violation constraint |
| $J_r$ | Rotor moment of inertia (kg-m$^2$) | $p_r$ | Belt drive ratio |
| $\boldsymbol{\omega}_{max}$ | Max motor speed (rad/s) | $mpg_e$ | Gasoline-equivalent fuel economy (mpg) |
| $B_I$ | Battery electrode thickness scale | $t_{60}$ | 0-60 time (s) |
| $B_W$ | Battery cell width scale | $\tau_V$ | Torque violation constraint |
| $B_L$ | Number of cell windings | $\boldsymbol{\omega}_V$ | Speed violation constraint |
| $b_m$ | Battery mass (kg) | $R$ | Vehicle range (mi) |
| $b_w$ | Battery width (m) | $P_V$ | Power availability constraint |
| $b_l$ | Battery length (m) | $C_b$ | Battery capacity (Ah) |
| $x_b$ | Battery compartment clearance (m) | | |

suspension trailing arms to minimize the unsprung mass in the system. The front suspension utilizes a MacPherson strut configuration, and finally, low rolling resistance P145/70R12 tires are included to minimize energy consumption.

Because this study only deals with powertrain design, the underlying analysis models experienced several changes (Alexander 2008). The structural design model, for example, was held constant and thus excluded from the problem. The powertrain analysis model was decomposed into three distinct entities: the electric motor, battery size, and vehicle-level analysis models. The remaining variables from the original powertrain analysis model (e.g., suspension variables) that were unaccounted for during decomposition have been treated as fixed parameters. The new analysis models are the following (Alexander 2008):

$$\begin{aligned}&\left[\mathbf{z}_{max},\ \mathbf{z}_{min},\ \mathbf{z}_{pLoss},\ J_r,\ \boldsymbol{\omega}_{max}\right]\\&\quad=\mathbf{f}_{motor}\left(l_s,\ r_m,\ n_c,\ R_r\right)\end{aligned}\tag{20}$$

$$\left[b_m,\ b_\ell,\ b_w\right]=\mathbf{f}_{battSize}\left(B_I,\ B_W,\ B_L\right)\tag{21}$$

$$\begin{aligned}&\left[m_s,\ \ell_1,\ h,\ I_y,\ I_z,\ b_{w,V},\ b_{\ell.V}\right]\\&\quad=\mathbf{f}_{evMass}\left(x_b,\ b_m,\ b_\ell,\ b_w\right)\end{aligned}\tag{22}$$

$$\begin{aligned}&\left[mpg_e, t_{60}, \tau_V, \boldsymbol{\omega}_V, R, P_V, C_b\right]\\&\quad=\mathbf{f}_v\left(B_I, B_W, B_L, b_m, m_s, I_y, \ell_1, \cdots\right.\\&\qquad\left. h, p_r, \mathbf{z}_{max}, \mathbf{z}_{min}, \mathbf{z}_{pLoss}, \boldsymbol{\omega}_{max}, J_r\right)\end{aligned}\tag{23}$$

The functions $\mathbf{f}_{motor}$, $\mathbf{f}_{battSize}$, $\mathbf{f}_{evMass}$, and $\mathbf{f}_v$ denote the electric motor, battery size, EV mass, and vehicle-level analysis models, respectively. Table 1 provides the definitions for the input/output quantities of each function, and Fig. 4 illustrates the relationships among the analysis models. Note that the dashed boxes in the figure indicate the problem decomposition for design optimization, which considers the interaction between the vehicle system and the motor subsystem.

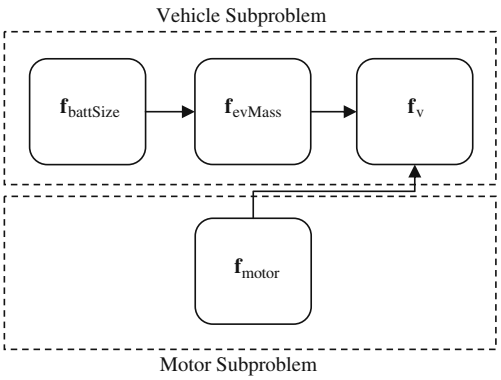


**Fig. 4** Analysis model relationships and problem decomposition

## 5 ATC problem formulation and results

The general ATC problem formulation for the EV powertrain system consists of a two-level hierarchical decomposition based on (3) and Fig. 4. The vehicle system objective is to maximize gasoline-equivalent fuel economy while minimizing the AL penalty function, whereas the motor subsystem objective is to minimize the AL penalty function exclusively. Both subproblems are subject to simple bound constraints; however, only the vehicle subproblem contains additional constraints based on packaging, performance, motor feasibility, power availability, and battery capacity.

Applying (3) directly, the vehicle subproblem $P_{11}$ (excluding simple bound constraints) is:

$$
\begin{aligned}
\min_{\bar{\mathbf{x}}_{11}} \; & -mpg_e\left(\bar{\mathbf{x}}_{11}\right) + \mathbf{v}_{22}^T\left(\mathbf{t}_{22} - \mathbf{r}_{22}\right) + \left\|\mathbf{w}_{22} \circ \left(\mathbf{t}_{22} - \mathbf{r}_{22}\right)\right\|_2^2 \\
\text{s.t.} \quad & g_{11,1}\left(\bar{\mathbf{x}}_{11}\right) = b_{w,V}\left(\bar{\mathbf{x}}_{11}\right) \le 0 \\
& g_{11,2}\left(\bar{\mathbf{x}}_{11}\right) = b_{\ell,V}\left(\bar{\mathbf{x}}_{11}\right) \le 0 \\
& g_{11,3}\left(\bar{\mathbf{x}}_{11}\right) = t_{60}\left(\bar{\mathbf{x}}_{11}\right) - t_{60max} \le 0 \\
& g_{11,4}\left(\bar{\mathbf{x}}_{11}\right) = \tau_V\left(\bar{\mathbf{x}}_{11}\right) \le 0 \\
& g_{11,5}\left(\bar{\mathbf{x}}_{11}\right) = \boldsymbol{\omega}_V\left(\bar{\mathbf{x}}_{11}\right) \le 0 \\
& g_{11,6}\left(\bar{\mathbf{x}}_{11}\right) = R_{min} - R\left(\bar{\mathbf{x}}_{11}\right) \le 0 \\
& g_{11,7}\left(\bar{\mathbf{x}}_{11}\right) = P_V\left(\bar{\mathbf{x}}_{11}\right) \le 0 \\
& g_{11,8}\left(\bar{\mathbf{x}}_{11}\right) = C_b\left(\bar{\mathbf{x}}_{11}\right) - C_{bmax} \le 0 \\
\text{where} \quad & \bar{\mathbf{x}}_{11} = \left[B_I,\ B_W,\ B_L,\ x_b,\ p_r,\ \mathbf{z}_{comb,r}^T,\ \boldsymbol{\omega}_{max}^T,\ J_r^T\right] \\
& \mathbf{t}_{22} = \left[\mathbf{z}_{comb}^T,\ \boldsymbol{\omega}_{max}^T,\ J_r^T\right], \mathbf{z}_{comb}^T = \mathbf{f}\left(\mathbf{z}_{comb,r}^T\right), \\
& \mathbf{r}_{22} = \left[\mathbf{z}_{comb}^R,\ \boldsymbol{\omega}_{max}^R,\ J_r^R\right]
\end{aligned}
\tag{24}
$$

Here, $g_{11,1}$ and $g_{11,2}$ are battery packaging constraints, $g_{11,3}$ is a performance (0–60 mph time) constraint, $g_{11,4}$ and $g_{11,5}$ are motor feasibility constraints, $g_{11,6}$ is a vehicle range constraint, $g_{11,7}$ is a power availability constraint, and $g_{11,8}$ is a battery capacity constraint (Allison 2008). It should be noted that $\mathbf{z}_{comb}$ and $\mathbf{z}_{comb,r}$ denote the original vector of combined VVCVs and the combined vector of reduced representation variables, respectively. Also, observe that the superscripts $T$ and $R$ denote target and response versions of the same coupling variable, respectively. Similarly, the motor subproblem $P_{22}$ (excluding simple bound constraints) is:

$$
\begin{aligned}
\min_{\bar{\mathbf{x}}_{22}} \; & \mathbf{v}_{22}^T\left(\mathbf{t}_{22} - \mathbf{r}_{22}\right) + \left\|\mathbf{w}_{22} \circ \left(\mathbf{t}_{22} - \mathbf{r}_{22}\right)\right\|_2^2 \\
\text{where} \quad & \bar{\mathbf{x}}_{22} = \left[\int_s,\ r_m,\ n_c,\ R_r\right] \\
& \mathbf{t}_{22} = \left[\mathbf{z}_{comb}^T, \boldsymbol{\omega}_{max}^T, J_r^T\right], \\
& \mathbf{r}_{22} = \left[\mathbf{z}_{comb}^R,\ \boldsymbol{\omega}_{max}^R,\ J_r^R\right] = \mathbf{f}\left(\bar{\mathbf{x}}_{22}\right)
\end{aligned}
\tag{25}
$$

The problem formulation shown in (24)–(25) was solved by implementing RBF ANN and POD separately as reduced representations of VVCVs associated with motor boundary torque curves and a power loss map. Due to the presence of non-smoothness in the powertrain model, a derivative-free optimization software package based on mesh-adaptive search algorithms known as NOMADm (Abramson 2007) was used. The settings for this MATLAB®-based optimizer were modified in the $P_{11}$ subproblem such that only a Latin hypercube search was performed and only 1,000 function evaluations were permitted. This was necessary to alleviate computational issues associated with memory availability. However, the default settings were appropriate in the $P_{22}$ subproblem. Note that identical starting points were used when optimizing the powertrain system for each reduced representation. Finally, the weight update parameter was set to $\boldsymbol{\beta} = 2.75$, the initial weight vectors were set to $\mathbf{v} = \mathbf{0}$ and $\mathbf{w} = \mathbf{1}$, and the tolerance on $||c^{(\mathrm{K})} - c^{(K-1)}||_\infty$ for outer loop convergence was set to $10^{-2}$.

### 5.1 Optimization results using RBF ANN

The optimization results using RBF ANN as a reduced representation technique are displayed in Tables 2 and 3. The

**Table 3** Optimal consistency constraint vector and penalty weights, ATC-RBF ANN

| Consistency constraint | $\mathbf{c}_{opt}$ | $\mathbf{v}_{opt}$ | $\mathbf{w}_{opt}$ |
|---|---|---|---|
| $c_{z,maz}$ | 1.54 | 669270 | 1189 |
| $c_{z,min}$ | 1.06 | 454402 | 1189 |
| $c_{z,pLoss}$ | 0.16 | 67422 | 1189 |
| $c_{\boldsymbol{\omega},max}$ | −0.15 | −65169 | 1189 |
| $c_{Jr}$ | 0 | 64.44 | 1189 |

**Table 2** Optimal decision vectors for vehicle and motor subproblems, ATC-RBF ANN

| Vehicle Subproblem, $P_{11}$ | | | | | | | | | | | Motor subproblem, $P_{22}$ | | | |
|---|---|---|---|---|---|---|---|---|---|---|---|---|---|---|
| $B_I$ | $B_W$ | $B_L$ | $x_b$ | $p_r$ | $l_s^T$ | $r_m^T$ | $n_c^T$ | $R_r^T$ | $\boldsymbol{\omega}_{max}^T$ | $J_r^T$ | $l_s^R$ | $r_m^R$ | $n_c^R$ | $R_r^R$ |
| 1.37 | 0.87 | 16.30 | 0.01 | 1.80 | 0.13 | 0.13 | 18.50 | 0.05 | 676 | 0.42 | 0.13 | 0.13 | 18.49 | 0.07 |

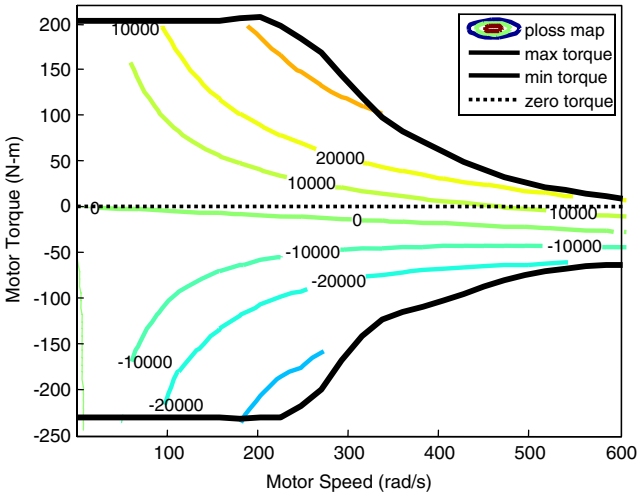


**Fig. 5** Optimal motor map, ATC-RBF ANN

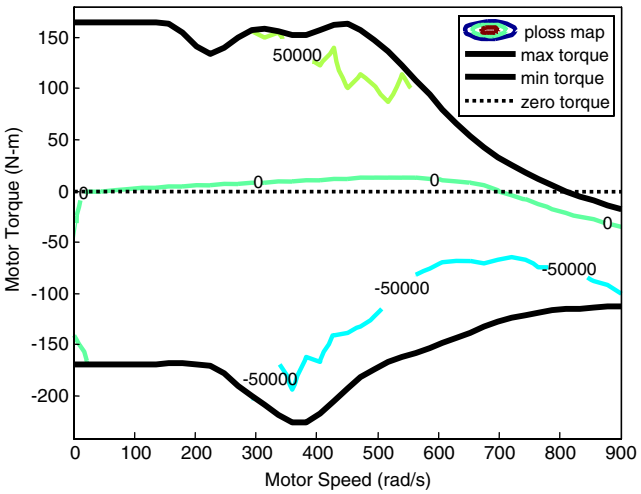


**Fig. 6** POD-approximated motor map at failed design point

algorithm successfully converged after 8 ATC iterations and resulted in a system solution that was consistent between both subproblems. In the vehicle subproblem, the bound constraint on $r_m^T$ and the performance constraint ($g_{11,3}$) were active; these values were limited to 0.13 m and 10 s, respectively. Such behavior was expected as maximizing fuel economy directly compromises vehicle performance. Similarly, the bound constraint on $r_m^R$ was active in the motor subproblem and therefore had the same value as in the vehicle subproblem. Implementing these design decisions along with the optimal motor map shown in Fig. 5, the optimizer predicts an EV with a gasoline-equivalent fuel economy of 236 mpg and a range of 160 miles.

## 5.2 Optimization results using POD

In implementing POD as a reduced representation technique during ATC, the algorithm initially failed due to a powertrain simulation crash. Figures 6 and 7 provide some insight regarding the cause of this failure. In particular, Fig. 6 illustrates that the POD approximation of the motor map was inaccurate, and Fig. 7 shows that the failed design point was outside the POD model validity region. Hence, the original assumption that the POD model validity region (and its design space) was defined by simple bound constraints was incorrect; instead, nonlinear constraints characterized the design space. Observe that Fig. 7 only captures a portion of this region graphically. Moreover, these variables lack physical meaning, making it challenging to formulate explicit constraints defining the model validity region. This issue is currently resolved by assigning large penalty values to objective and constraint function outputs that depend on the reduced representation variables when simulation failure occurs. For non-gradient-based optimizers, this can be effective as it forces the selection of reduced representation variables that lie within the model validity region. It should be noted that other methods, such as support vector domain description (Tax and Duin 1999a, b), have been explored to resolve this issue (Alexander et al. 2010b); however, more work is necessary to determine the suitability of SVDD compared to the current, penalty value-based approach (Alexander and Papalambros 2010).

The optimization problem was attempted again while implementing this constraint management heuristic through a "try-catch" statement in MATLAB® (MATLAB® Function Reference). Convergence was achieved after 83 ATC iterations and resulted in a system solution that was consistent between both subproblems, as indicated in Tables 4 and 5. The optimal values of the reduced representation

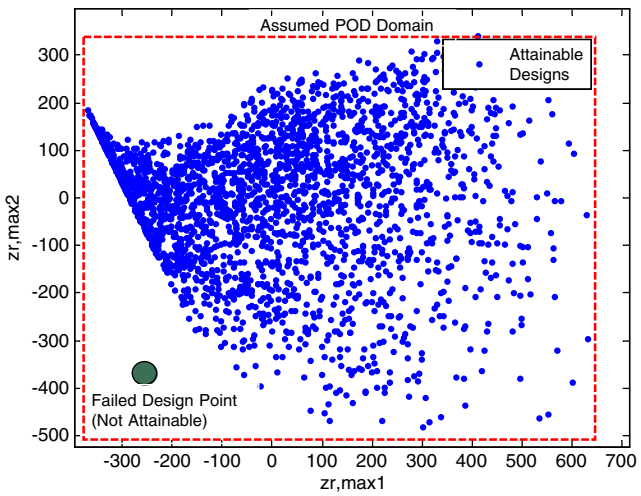


**Fig. 7** POD model validity region for two components

**Table 4** Optimal decision vectors for vehicle and motor subproblems, ATC-POD

| Vehicle subproblem, $P_{11}$ | | | | | | | Motor subproblem, $P_{22}$ | | | |
|---|---|---|---|---|---|---|---|---|---|---|
| $B_I$ | $B_W$ | $B_L$ | $x_b$ | $p_r$ | $\omega_{max}^T$ | $J_r^T$ | $l_s^R$ | $r_m^R$ | $n_c^R$ | $R_r^R$ |
| 0.84 | 1.08 | 22.70 | 0.03 | 2.12 | 676 | 0.42 | 0.13 | 0.13 | 18.36 | 0.14 |

variables are not listed here as they are not physically meaningful; however, the optimal motor map computed by these variables is shown in Fig. 8. The only activity in the vehicle subproblem was the battery width ($g_{11,1}$) and capacity ($g_{11,8}$) constraints, which were limited to 1.20 m and 200 Ah, respectively. Such a solution was not unrealistic but somewhat unusual given that performance usually dominates the other constraints in this problem. A likely cause of this phenomenon was the larger inconsistency in $c_{pLoss}$ for POD compared to RBF ANN. In the motor subproblem, the bound constraint on $r_m^R$, which was limited to 0.13 m, was active again. Implementing these design decisions, the optimizer predicts an EV with a gasoline-equivalent fuel economy of 217 mpg, a 0–60 mph time of 8.5 s, and a range of 130 miles.

## 6 Efficiency and accuracy assessment

The efficiency of each reduced representation was assessed in terms of three criteria: dimensionality reduction of the vehicle subproblem $P_{11}$, computational expense incurred while constructing the reduced representations, and computational expense incurred while performing ATC optimization. Based on Sections 3.1 and 3.2, it is evident that RBF ANN outperformed POD in terms of dimensionality reduction. When using RBF ANN, $P_{11}$ consisted of 5 local design variables, 4 reduced representation variables, and 2 additional coupling variables, yielding an overall dimensionality of 11. POD required 123 reduced representation variables, resulting in an overall dimensionality of 130 for $P_{11}$. However, when comparing the computational expense in constructing the reduced representations, it was observed that POD was much more efficient. The runtime for POD was 46.05 s, whereas the runtime for RBF ANN was $3.32 \cdot 10^4$ s (∼9.2 h). The key factor that extended the runtime for RBF ANN was an optimization subroutine that was performed to identify the optimal $b_h$ for each network. Nevertheless, when comparing the computational expense while performing optimization, RBF ANN was more efficient. The runtime for RBF ANN was $2.91 \cdot 10^4$ s (∼8.1 h), whereas the runtime for POD was $2.12 \cdot 10^5$ s (∼59 h). Therefore, the total runtimes for RBF ANN and POD were $6.23 \cdot 10^4$ s (∼17.3 h) and $2.12 \cdot 10^5$ s (∼59 h), respectively. All computational work was performed on a 3 GHz, 4 GB RAM, Intel® Core™ 2 Duo CPU. Using these aggregate runtimes and considering $P_{11}$ subproblem dimensionality, it is clear that RBF ANN was the least computationally expensive reduced representation technique.

The accuracy and validity algorithm for simulation, or AVASIM (Sendur et al. 2002), was used to assess the accuracy of each reduced representation. This error metric measures the local and global error between functional data and their approximations through $l_1$-norms and residual sums. Error indices are developed using these measures such that nonnegative values of the combined index denote

**Table 5** Optimal consistency constraint vector and penalty weights, ATC-POD

| Consistency constraint | $c_{opt}$ | $v_{opt}$ | $w_{opt}$ |
|---|---|---|---|
| $c_{z,maz}$ | 0.72 | $2.46 \times 10^{71}$ | $1.06 \times 10^{36}$ |
| $c_{z,min}$ | 0.70 | $2.41 \times 10^{71}$ | $1.06 \times 10^{36}$ |
| $c_{z,pLoss}$ | 1.80 | $6.05 \times 10^{71}$ | $1.06 \times 10^{36}$ |
| $c_{\omega,max}$ | −0.13 | $-4.53 \times 10^{70}$ | $1.06 \times 10^{36}$ |
| $c_{Jr}$ | 0 | $-4.30 \times 10^{68}$ | $1.06 \times 10^{36}$ |

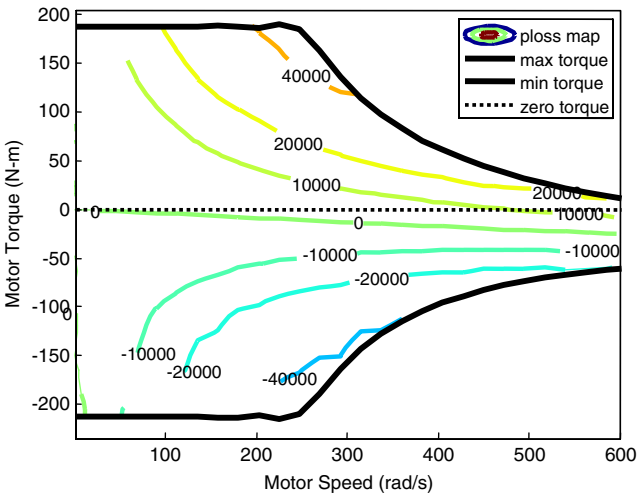


**Fig. 8** Optimal motor map, ATC-POD

**Table 6** AVASIM results

| Index | RBF ANN | | | POD | | |
|---|---|---|---|---|---|---|
| | $z_{max}$ | $z_{min}$ | $z_{pLoss}$ | $z_{max}$ | $z_{min}$ | $z_{pLoss}$ |
| $E_{local}$ | −17.00 | −0.46 | −380.62 | 0.36 | 0.84 | −203.28 |
| $E_{global}$ | −0.44 | 0.18 | − 0.43 | 0.82 | 0.84 | 0.82 |
| $E_{comb}$ | −8.72 | −0.14 | −190.53 | 0.59 | 0.84 | −101.23 |

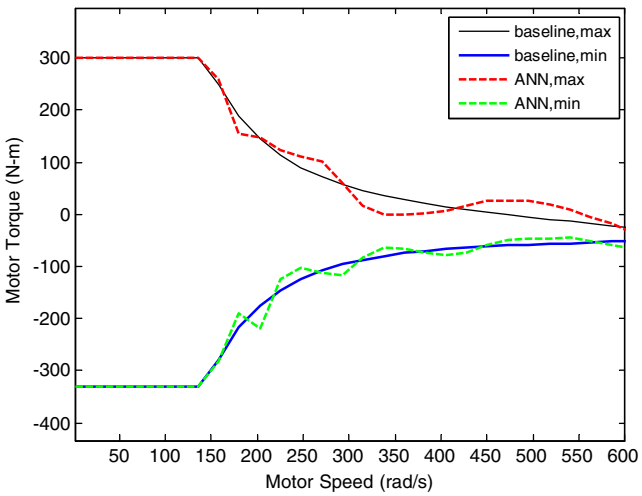


**Fig. 9** Torque curve comparison, RBF ANN approximation and baseline

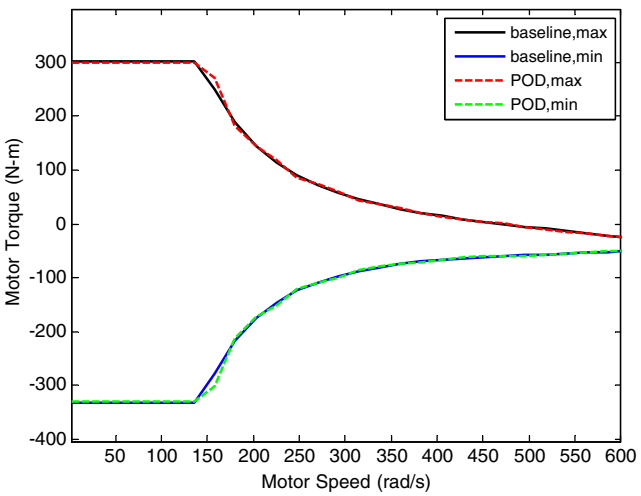


**Fig. 11** Torque curve comparison, POD approximation and baseline

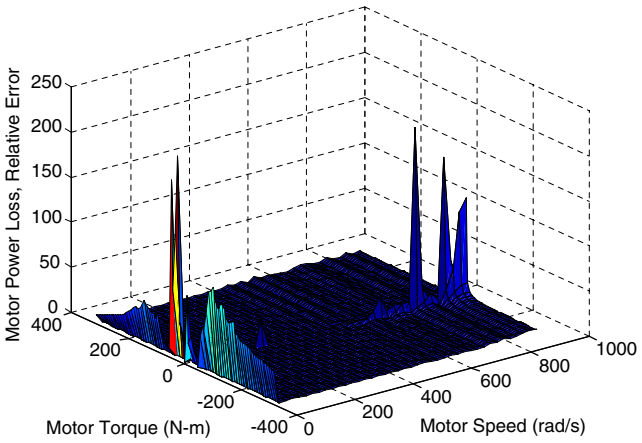


**Fig. 10** Power loss map relative error, RBF ANN approximation and baseline

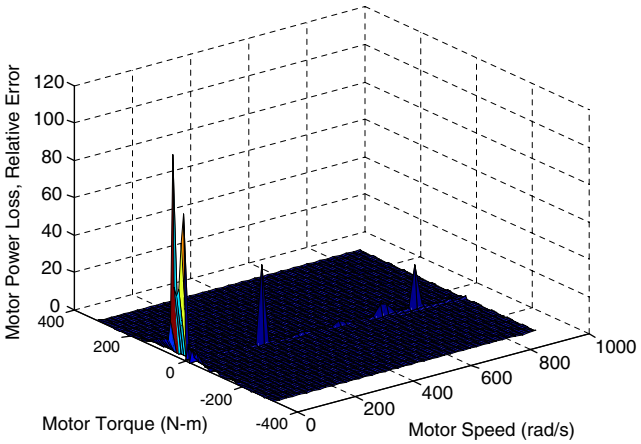


**Fig. 12** Power loss map relative error, POD approximation and baseline

valid approximations with accuracy levels between 0 and 1, and all negative values of the combined error index denote invalid approximations. Note that validity is defined by approximations that lie within a preset threshold value; therefore, a value of 0 indicates that an approximation is at the threshold and valid, whereas a value of 1 indicates that an approximation is completely accurate. Because this study required the accuracy assessment of power loss maps, which are two-dimensional functional data, an extended version of AVASIM had to be implemented (Alexander and Papalambros 2010). In addition, since the global behavior of the approximations is much more important than the local behavior (which influences the combined index), the most meaningful error measure in this work is the global index. AVASIM was applied with a 10% tolerance to quantify the accuracy of the torque curves and power loss maps produced by RBF ANN and POD against optimal torque curves and power loss maps produced by the corresponding all-in-one (AiO) optimization problem. Table 6 shows the results from AVASIM and Figs. 9, 10, 11, 12 illustrate the accuracy of the reduced representations visually. Based on these observations, it is clear that POD was a more accurate reduced representation than RBF ANN.

## 7 Conclusions and future work

Although each reduced representation method has its own merit, there is a significant amount of evidence to suggest that POD is the best approach for this study. The most compelling reason is that the ATC-RBF ANN formulation does not satisfy the necessary condition of additive-separability for decomposition-based optimization strategies. In particular, the decision vector in the motor subproblem $P_{22}$ is identical to the reduced representation variables in the vehicle subproblem $P_{11}$, which implies that $P_{22}$ is not unique and should be incorporated into $P_{11}$. This further implies that an AiO formulation should have been used to solve the optimization problem, which was not the goal of this study. Conversely, POD easily satisfies additive-separability as it uses reduced representation variables that are physically meaningless and unlikely to be used elsewhere in a decomposition-based optimization strategy. In the event that additive-separability is satisfied, another limitation of RBF ANN is that the number of reduced representation variables is not always guaranteed to be less than the dimensionality of the original VVCV. This issue was not relevant in the current study, but could pose problems in larger, more complex system design studies. POD, however, is guaranteed to generate reduced representations that have a lower dimension than the original VVCV by virtue of its process. A final limitation of RBF ANN (assuming additive-separability is satisfied) is its lack of flexibility. Regardless of the desired accuracy, the number of reduced representation variables is always equal to the number of inputs to the network. This is not the case for POD; the number of reduced representation variables is directly related to the CPV, which allows for tremendous flexibility. Specifically, POD enables a tradeoff between "accuracy" (although strictly speaking, CPV does not measure accuracy) and dimensionality reduction through the CPV, whereas RBF ANN (as implemented) does not have this capability.

In general, the limitations for RBF ANN could exist for any reduced representation; however, it is seen that metamodeling approaches frequently risk experiencing these issues as they use physically meaningful variables that are not guaranteed to reduce problem dimensionality and may violate additive-separability. Hence, RBF ANN and similar methods are best suited for decomposition-based design optimization problems in which these conditions are met. In the event that additive-separability and dimensionality reduction are not satisfied, curve-fitting approaches such as POD would be more appropriate for decomposition-based design optimization because they use abstract variables that are guaranteed to reduce problem dimensionality and are unlikely to violate additive-separability. POD is among the most attractive of these curve-fitting approaches as it generates a functional form without prior user assumptions, makes limited assumptions regarding the number of fitting parameters, and uses a relatively small number of fitting parameters for the VVCV approximations based on data samples. Despite the advantages, however, a key practical issue that must be addressed is the constraint management of the POD model validity region. The MATLAB® "try-catch" statement is effective but not efficient as it requires many ATC iterations that can lead to an ill-conditioned optimization problem and extensive runtimes. Ideally, the POD model validity region should be constrained using a more direct method that utilizes explicit constraints in the optimization formulation. This would enable the optimizer to perform more efficiently and lead to fewer ATC iterations and faster runtimes. Methods such as SVDD that are beginning to be explored (Alexander et al. 2010b) may offer a suitable alternative that also makes use of the known, attainable designs shown in Fig. 7. The thorough investigation of such an approach is a topic proposed for future work.

**Acknowledgments** This research was partially supported by the Automotive Research Center, which is a U.S. Army Center of Excellence at the University of Michigan. It was also funded by the U.S. National Consortium for Graduate Degrees for Minorities in Engineering and Science, Inc., as well as a University of Michigan Rackham Merit Fellowship. This support is gratefully acknowledged.

## References


Abramson MA (2007) NOMADm version 4.5 user's guide. Air Force Institute of Technology, Wright-Patterson AFB, OH

Ahmed N, Goldstein MH (1975) Orthogonal transforms for digital signal processing. Springer, Berlin

Alexander MJ (2008) Analytical target cascading optimization of an electric vehicle powertrain system. Thesis, University of Michigan

Alexander MJ (2011) Management of functional data variables in decomposition-based design optimization. Dissertation, University of Michigan

Alexander MJ, Papalambros, PY (2010) An accuracy assessment method for two-dimensional functional data in simulation-based design. In: Proceedings of the 13th AIAA/ISSMO multidisciplinary analysis and optimization conference, Fort Worth, TX

Alexander MJ, Allison JT, Papalambros, PY (2009) Reduced representations of vector-valued coupling variables in decomposition-based design optimization. In: Proceedings of the 8th world congress on structural and multidisciplinary optimization, Lisbon, Portugal

Alexander MJ, Allison JT, Papalambros PY (2010a) Decomposition-based design optimization of electric vehicle powertrains using proper orthogonal decomposition. Int J Powertrains (in press)

Alexander MJ, Allison JT, Papalambros PY, Gorsich DJ (2010b) Constraint management of reduced representation variables in decomposition-based design optimization. In: Proceedings of the 2010 ASME international design engineering technical conferences, Montreal, Canada, DETC2010-28788

Allison J (2008) Optimal partitioning and coordination decisions in decomposition-based design optimization. Dissertation, University of Michigan

Box GEP, Draper NR (1987) Empirical model-building and response surfaces. Wiley, New York

Box GEP, Hunter JS (1957) Multi-factor experimental designs for exploring response surfaces. Ann Math Stat 28:195–241

Bretscher O (2005) Linear algebra with applications, 3rd edn. Pearson Prentice Hall, Upper Saddle River

Bui-Thanh T, Damodaran M, Wilcox K (2004) Aerodynamic reconstruction and inverse design using proper orthogonal decomposition. AIAA J 42(8):1505–1516

Burkhardt J, Du Q, Gunzburger M, Lee HC (2003) Reduced order modeling of complex systems. In: Proceedings of the 20th biennial conference on numerical analysis, Dundee, Scotland

Chen S, Cowan CFN, Grant PM (1991) Orthogonal least squares learning algorithm for radial basis function networks. IEEE Trans Neural Netw 2(2):302–309

Demuth H, Beale M, Hagan M (2009) MATLAB® neural network toolbox™ version 6 .0.2 user's guide. The MathWorks, Inc., Natick

George P, Ogot MM (2006) A compromise experimental design method for parametric polynomial response surface approximation. J Appl Stat 33(10):1037–1050

Glasbey CA, Mardia KV (1998) A review of image warping methods. J Appl Stat 25(2):155–172

Karhunen K (1946) Zur spektral theorie stochastischer prozesse. Ann Acad Sci Fen 34

Kim HM (2001) Target cascading in optimal system design. Dissertation, University of Michigan

Kim HM, Michelena NF, Papalambros PY, Jiang T (2003) Target cascading in optimal system design. ASME J Mech Des 125(3):474–480

Kokkolaras M, Louca LS, Delagrammatikas GJ, Michelena NF, Filipi ZS, Papalambros PY, Stein JL, Assanis DN (2004) Simulation-based optimal design of heavy trucks by model-based decomposition: an extensive analytical target cascading case study. Int J Heavy Veh Syst 11(3–4):402–431

LeGresley PA, Alonso JJ (2004) Improving the performance of design decomposition methods with POD. In: Proceedings of the 10th AIAA/ISSMO multidisciplinary analysis and optimization conference, Albany, NY, AIAA 2004–4465

Loeve M (1945) Functions aleatoire de second ordre. C R Academie des Sciences, Paris

Lucia DJ, Beran PS, Silva WA (2003) Reduced order modeling: new approaches for computational physics. Prog Aerosp Sci 40: 51–117

Meade AJ, Kokkolaras M (1996) Enhancement of a viscous-inviscid-interaction airfoil analysis code using the parallel direct search algorithm. Technical report CRPC TR96711-S. Rice University

Sansone G, Hille E (2004) Orthogonal functions, revised English ed. Dover, Mineola

Sendur P, Stein JL, Louca LS, Peng H (2002) A model accuracy and validation algorithm. In: Proceedings of the ASME international mechanical engineering congress and exposition, New Orleans, LA

Sirovich L (1987) Turbulence and the dynamics of coherent structures. I – coherent structures. II – symmetries and transformations. III – dynamics and scaling. Quart Appl Math 43:561–571–573–590

Sobieski I, Kroo I (1996) Aircraft design using collaborative optimization. In: Proceedings of the AIAA 34th aerospace sciences meeting and exhibit, Reno, NV

Stegmann MB (2001) Image warping. Technical report. Technical University of Denmark

Tax DMJ, Duin RPW (1999a) Data domain description using support vectors. Proceedings of the european symposium on artificial neural networks. Bruges, Belgium, pp 251–256

Tax DMJ, Duin RPW (1999b) Support vector domain description. Pattern Recognit Lett 20:1191–1199

Toal DJJ, Bressloff NW, Keane AJ (2008) Geometric filtration using POD for aerodynamic design optimization. In: Proceedings of the 26th AIAA applied aerodynamics conference. Honolulu, HI, AIAA, pp 2008–6584

Tosserams S, Etman LFP, Papalambros PY, Rooda JE (2006) An augmented Lagrangian relaxation for analytical target cascading using the alternating direction method of multipliers. Struct Multidiscip Optim 31:176–189

Wagner TC, Papalambros PY (1993) A general framework for decomposition analysis in optimal design. In: ASME advances in design automation, vol 65. Albuquerque, NM, pp 315–325

Wilcox K (2005) An introduction to model reduction for large scale applications. In: Aerospace computational design laboratory seminar, http://web.mit.edu/mor/papers/ADCL_Sept05.pdf. Massachusetts Institute of Technology